Relationship between Enzyme Specificity and the Backbone Dynamics of Free and Inhibited α-Lytic Protease[†,‡]

Jonathan H. Davis[§] and David A. Agard*

Graduate Group in Biophysics, Howard Hughes Medical Institute, and Department of Biochemistry and Biophysics, University of California, San Francisco, 513 Parnassus Avenue, San Francisco, California 94143-0448

Received December 2, 1997; Revised Manuscript Received March 26, 1998

ABSTRACT: To better understand the structural basis for the observed patterns in substrate specificity, the backbone dynamics of α-lytic protease have been investigated using ^{15}N relaxation measurements. The enzyme was inhibited with the peptide boronic acid *N-tert*-butyloxycarbonyl-Ala-Pro-boroVal [Kettner, C. A., et al. (1988) *Biochemistry 27*, 7682], which mimics interactions occurring in the tetrahedral transition state or nearby intermediates, and the dynamics of the unbound and inhibited enzyme were compared. Arrayed 2-D NMR spectra were acquired to measure T_1, T_2, and steady-state $\{^1H\}-^{15}N$ NOE of >95% of the backbone amides in both protein samples. The overall rotational correlation time τ_c was found to be 8.1 ns. Values of the spectral density function $J(\omega)$ at $\omega = 0$, ω_N, and $\sim\omega_H$ were derived from the relaxation results using reduced spectral density mapping [Ishima, R., & Nagayama, K. (1995) *Biochemistry 34*, 3162]. The resultant spectral densities were interpreted to indicate regions of fast motion (nanosecond to picosecond) and of intermediate chemical exchange (millisecond to microsecond). The protein has 13 regions with increased motion on the fast time scale; these generally fall on exterior turns and loops and most correlate with regions of higher crystallographic *B*-factors. Several stretches of backbone undergo intermediate chemical exchange, indicating motion or other processes that cause temporal chemical shift changes. A comparison of spectral densities for both the free and inhibited enzymes revealed that inhibitor binding preferentially stabilizes regions undergoing chemical exchange (which predominate around the active site) and only minimally affect regions of rapid motion. Slow motions, suggestive of backbone plasticity, are observed in most of the binding pocket residues. This may point to a mechanism for the observed broad specificity of the enzyme. The significance of the observed dynamics for substrate binding and specificity is discussed.

While crystal structures of enzymes bound to substrate and transition state analogues have helped to determine the reactive mechanisms and binding sites for many enzymes, the detailed structural basis for the observed patterns of substrate specificity is largely unknown. Fundamental to understanding specificity is the analysis of how a variety of substrates can be accommodated by the enzyme. Such accommodations may rely on dynamic properties of the enzyme binding pocket, which cannot be readily appreciated through crystallographic analyses. Although the exact role played by dynamics in enzyme specificity and catalysis is unknown, it is generally believed to be important (*1*, *2*), and the idea of a dynamical "induced fit" has been widely discussed (*3*). In those cases where an induced fit model of substrate binding applies, one might expect substrate (or analogue) binding to alter the dynamics of the region involved in contacting the substrate. NMR relaxation can probe the dynamic behavior of individual protein sites, and several proteins have been studied both free and bound to a ligand. While in some studies the active site was found to be stabilized by ligand binding (*4*−*6*), in other studies the results were mixed (*7*). Thus, the relationship between enzyme dynamics and substrate binding is not obvious, and further study may be illuminating.

A central focus of our laboratory's research has been to understand the structural basis for an enzyme's observed pattern of substrate specificity. Toward this end we have combined X-ray crystallography, mutagenesis, kinetic analysis, and now NMR dynamics studies to probe structure−function relationships using α-lytic protease (α-LP)[1] as a model system. α-LP is an extracellular bacterial serine protease of the chymotrypsin family produced by the soil bacterium *Lysobacter enzymogenes*. The mature form consists of 198 residues, and its crystal structure has been solved to 1.7 Å resolution at room temperature (*8*) and to 1.5 Å at 120 K (*9*). α-LP has been an excellent model enzyme for studies of structure−function relationships (*10*−*16*) and has been extensively studied to understand its unusual thermodynamics (*17*) and its requirement of a pro region for proper folding (*17*−*19*).

[†] This work was supported by the Howard Hughes Medical Institute.

[‡] This paper is dedicated to the memory of Bernard D. Davis.

* To whom correspondence should be addressed.

[§] Current address: Department of BCMP, Harvard Medical School, 240 Longwood Ave., Boston, MA 02115.

[1] Abbreviations: α-LP, α-lytic protease; HSQC, heteronuclear single-quantum coherence; NOE, nuclear Overhauser effect; RSDM, reduced spectral density mapping; CPMG, Carr−Purcell−Meiboom−Gill sequence; FID, free induction decay; Boc, *N-tert*-butyloxycarbonyl; BVal, borovaline. Standard abbreviations are used for amino acids.

S0006-2960(97)02963-2 CCC: $15.00
Published on Web 05/07/1998

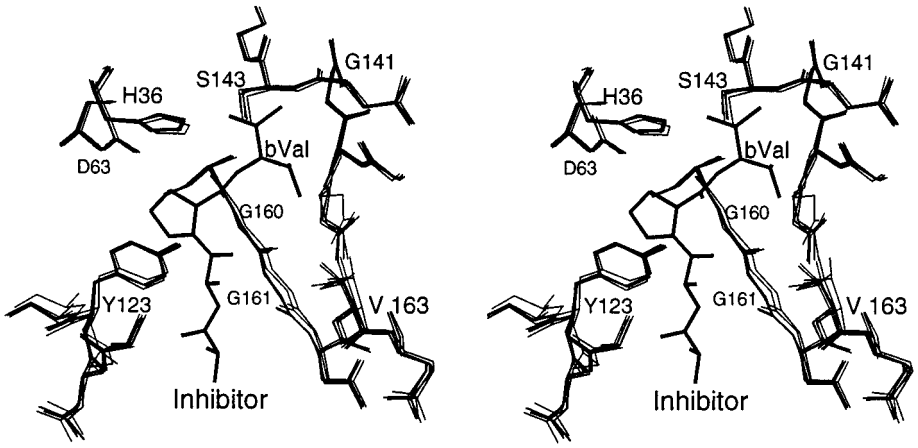

FIGURE 1: Stereoview of the overlay of five globally matched crystal structures, showing the flexibility of the active site upon binding different inhibitors. Shown is one boronic acid inhibitor, Ala-Ala-Pro-boroVal; the other four protein structures are bound with A-A-P-boroAla, -boroLeu, -boroIle, and -boroPhe (inhibitors not shown). The backbone shifts to accommodate the different sized P_1 side chains. The regions of greatest apparent backbone flexibility are G160−V163 and N122−Y123. Figures such as this one (*13*) raised the questions regarding active site flexibility and dynamics addressed in this study.

Key to our structural studies has been the use of potent peptide inhibitors that allow us to examine interactions that might occur in the reaction transition state or in nearby tetrahedral intermediates. Among the most useful inhibitors has been a set of peptide boronic acids (*20*, *21*) having different amino acid side chains in the specificity-determining position (*13*). Crystallographic analysis of a number of point mutations in the binding pocket which resulted in both high activity and extremely broad specificity indicated that the protease has a remarkable ability to adjust conformation to optimally accommodate substrates. When a set of such highly refined structures corresponding to different combinations of mutants and inhibitors are superimposed using all Cα coordinates, some residues in the binding pocket are displaced, while others remain superimposable (see Figure 1) (*9*, *12*, *13*). Although such pictures actually represent static views of discrete enzyme−inhibitor complexes, they are quite suggestive of dynamic motion. By contrast, in each of the individual structures, the small crystallographic *B*-factors observed in the binding region suggest rigidity. A fundamental question is whether the enzyme conformations observed in the discrete complexes are within an envelope that are dynamically sampled by the uncomplexed native enzyme. If so, then we would expect to see a correlation between the regions that show the most conformational variation on ligand binding and those that show increased dynamics in the uncomplexed protein. Nature has optimized α-LP to have specificity for small hydrophobic residues at the cleavage site, and the enzyme's presumed purpose is the general digestion of proteins in other microorganisms and the soil. Thus, there is good reason for the specificity at the other sites contacting the substrate to be broad (as is also found in the digestive enzymes chymotrypsin, elastase, and trypsin). Binding pocket flexibility may be key for limiting specificity to the single residue occupying the P_1[2] site and allowing the induced fit to a wide variety of substrate sequences.

NMR relaxation measurements have been used successfully to study the dynamic nature of protein backbones for motions ranging from milliseconds to picoseconds (*2*, *22*). ^{15}N relaxation probes the motions of the backbone NH bond vector and can indicate motions both faster and slower than the overall rotational correlation time τ_c. In this study we use a reduced spectral density mapping (RSDM) method (*23*−*29*) to analyze the ^{15}N relaxation of backbone amides in native α-LP, both alone and complexed with the peptide transition state mimic *N-tert*-butyloxycarbonyl-Ala-Pro-boroVal (Boc-Ala-Pro-BVal, K_i = 0.35 nM) (*21*). The analysis was performed with ^{15}N T_1, T_2, and {^{1}H}−^{15}N NOE (cross-relaxation) rates measured at a proton frequency of 600 MHz. We were particularly interested in observing motions that changed upon inhibitor binding.

MATERIALS AND METHODS

Sample Preparation. ^{15}N-Labeled α-LP was produced using the native host *L. enzymogenes* and purified as described previously (*30*, *31*), using ^{15}N-labeled glutamic acid (Cambridge Isotopes Laboratories) and ^{15}N-labeled Celtone (Martek). Purified enzyme was dissolved in H_2O buffer containing 40 mM deuterated sodium acetate, 40 mM sodium chloride, and 7% D_2O, pH 4.0, and then concentrated in a Centricon filter (Amicon) to a volume of 250 μL, with a final concentration of 2.5−3.0 mM. The sample was then placed into a reduced-volume NMR tube (Shigemi). Samples were repurified for each stretch of instrument time used. The inhibitor complex sample was prepared the same way, except that before the final concentration step inhibitor was added until measured activity decreased below the detection limit; then the pH was adjusted to 4.0. The estimated concentration of the inhibited sample was 2.0 mM. Samples were degassed in the tube by using the plunger to create a partial vacuum and extract the bubbles, while running N_2 over the top of the tube.

NMR Spectroscopy. All experiments were recorded at 35 °C on a Varian Unity-plus 600 MHz spectrometer equipped with a triple-resonance gradient probe. The pulse sequences used combine features from those published by Farrow et al. (*7*) and Farrow et al. (*24*), including semiconstant time (*32*−*34*). We did not use extra shaped pulses to prevent water saturation, since at pH 4.0 there is minimal exchange with solvent. An additional element allows the experiments to be arrayed (see below).

[2] In protease substrate nomenclature, the amino acid residue to the amino-terminal side of the scissile bond is referred to as the P_1 position, and numbers increase toward the N-terminus of the substrate.

T_1 and T_2 spectra were acquired with 1K × 128 complex points and spectral widths of 10 000 and 2460 Hz in t_2 and t_1, respectively. Each FID contained 16 scans, and 64 dummy scans preceded the experiment. For the T_1 measurements, delays of 16, 64, 128, 224, 336, 480, 720, 1008, and 1440 ms were arrayed, and the shortest delay was repeated for error estimation. The phase cycling was arranged to cause the T_1 magnetization to relax to zero (*35*). The relaxation delay between scans was 1.5 s (free enzyme) and 1.4 s (inhibited enzyme). The T_2 measurement on the native protein used 0, 14, 28, 42, 56, 70, 84, 113, and 141 ms delays, and the T_2 measurement on the BVal complex used 8.6, 17.3, 34.6, 51.8, 69.1, 86.4, 112.3, and 138.2 ms delays. Nonarrayed T_2 experiments with similar relaxation delays were also performed with a 2.0 ms delay between CPMG pulses. The relaxation delay between scans was 1.3 s for all T_2 experiments. The steady-state NOE measurement was an arrayed experiment with 1K × 170 complex points in t_2 and t_1, the same spectral widths as above, and 32 scans per FID. Two dummy scans preceded each FID to ensure that no residual saturation was passed from the saturated scans to the control scans in the array. The system was allowed to relax for 3.7 s between FIDs, about 4 times the longest ^{15}N T_1. At pH 4 there is no significant exchange between water and amides in the time scale of this experiment, so problems associated with residual saturated water exchanging with amides were negligible. For the saturated experiment, a series of 120° ^{1}H pulses with 5 ms delay between them was applied for the final 3.0 s of the relaxation delay. To minimize heating, which could affect the rapid motions to which the NOE is particularly sensitive, the transmitter power was reduced 6 dB during this period.

Spectra were processed using nmrPipe (*36*, *37*). A typical processing scheme is as follows: application of a Lorentz-to-Gauss window function with 10 Hz inverse exponential and 17 Hz Gaussian line broadening and zero-filling to 4K complex points prior to transforming the t_2 dimension, and then complex linear prediction of 96 points in t_1 followed by a Lorentz-to-Gauss transformation with a 4.5 Hz inverse exponential and 11 Hz Gaussian line broadening and zero-filling to 1K complex points. Baseline correction with polynomial order 2 or 3 was performed in both dimensions after the final Fourier transform. The Lorentz-to-Gauss transformations used in both dimensions ensured excellent fits to 2-D Gaussian functions in the data analysis, even for rather badly overlapped peaks.

The processed 2-D spectra were displayed and analyzed using the in-house program Sparky[3] (D. Kneller, unpublished). Peaks were fit to a two-dimensional Gaussian using the simplex method of Nelder and Mead (*38*). The height of the fitted curve was then extracted for the intensity of the peak. The fitted height yielded the lowest error value (error ≈ ±0.3% on the strongest spectrum, ±3% on the weakest, somewhat less than the RMSD noise level of the spectra), since it is less sensitive than volume to slight line width variations caused by noise but also less sensitive than the simple peak height to noise and overlap. T_1 and T_2 relaxation rates were generated by fitting the heights to a single exponential decaying to zero using a Levenburg−Marquardt algorithm (*38*). Monte Carlo simulations were used to estimate the actual error of the fits given the error in the heights (*38*, *39*), with 500 simulations per fit. The maximum NOE was calculated by taking the ratio of the saturated intensities vs the control intensities. In all cases the standard error of the intensities was determined by comparing duplicate spectra and dividing the standard deviation of matched peaks by $\sqrt{2}$ (*40*).

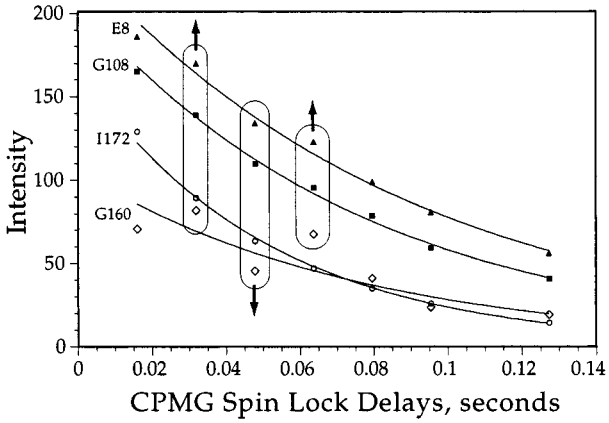

FIGURE 2: Exponential fits to T_2 data of free α-LP that was collected parametrically but not arrayed and with a 2 ms delay between CPMG ^{15}N 180° pulses. Though the fits are quite poor for determining relaxation rates, the scatter in the data is not random but comes from the decaying sample. The time point at 0.064 s was the first collected, 0.032 was second, and 0.048 was last. Much of the protein looked like G108 (solid squares) or with even less pronounced variation (but with a similar pattern). But closer to the active site, some residues showed exaggerated effects, e.g., E8 (triangles, <12 Å from the inhibitor) and G160 (diamonds, 4 Å away). The effect is caused by the slow deterioration of the protein over the experimental period and, when exaggerated, indicates the presence of chemical exchange caused by peptide binding. I172 (circles) shows only random deviation from its exponential fit, even though it has a high component of chemical exchange, strongly suggesting that the exchange contribution is from motion, not peptide binding.

Arrayed Experiments. α-LP is an ideal molecule for NMR studies in many ways (e.g., peak dispersion, homogeneity of structure, and solubility), but it has some serious drawbacks for dynamics measurements. Being a potent protease, it slowly autolyses and can lose up to 1% per day when at NMR concentrations and 35 °C. Therefore, the sample inevitably changes over the course of a ∼24 h relaxation experiment, causing systematic errors in the NMR spectra. T_1 peak intensities varied above or below the exponential fit by up to 1−2% according to the order in which they were collected. In the T_2 experiments this same pattern occurred except that, for some residues, the deviations were much greater (see Figure 2). The residues with exaggerated errors are all very close to the binding site, and most have shortened T_2's. These results suggest that there is slow degradation of the sample over the 24 h of data collection, and the resulting proteolytic products, which would be a collection of short peptides, build up at a much faster rate (on a molar basis). Any site where peptide binding occurs would have a shorter T_2 decay, due to the exchange broadening caused by peptide binding and release. Experience with α-LP indicates that proteolysis leads to the rapid production of short peptides that should have no well-defined tertiary structure. Quite unusual conditions are required to generate large cleavage products that may be partially structured (J.

[3] For software availability, please contact Dr. I. D. Kuntz, UCSF, Box 0446, San Francisco, CA 94143-0446.

Tamm, Clorox Corp., personal communication). NMR spectra support this as well; any cleavage that allowed stable fragments should also cause a distinct alteration in chemical shift at one or more residues. No such peak splittings are observed; however, small sharp peaks do appear in the central region of the amide correlation spectrum, as would be expected from the production of short peptides. The N and C termini are protected from proteolysis in the native enzyme, and with the exception of a broadened line for the amide of N2 (which could be the result of multiple conformations), there is no evidence for terminal heterogeneity.

To eliminate the systematic errors in the T_2 relaxation spectra, we arrayed the experiments such that, for any given relaxation measurement, all the 2-D spectra were collected in parallel over the entire ~24 h of measurement. In the arrayed experiment, sample changes affect all the spectra equally and are reflected only in line shape changes. There is a negligible effect on the calculated rates because for a given amide all time points have the same line shape, so the true intensity relationships between the peaks are maintained. A bonus we gained from this approach was a clear indication of whether chemical exchange was caused by peptide binding or by motion. Comparison of arrayed and nonarrayed exponential fits gave a clear indication of sites where peptide binding contributed to the chemical exchange terms. To allow shorter predelays without significant deviations from the steady state as the array progressed, all proton magnetization was killed with a pulse/gradient sequence before the predelay.

The problem of degradation affects the NOE experiment in a more severe manner; any buildup of peptides produces peaks that are small and positive in the control experiment and stronger and negative in the saturated experiment, due to their very short correlation times. In the case of superposition of a peptide peak with a protein peak, this leads to an artificially small ratio I_{sat}/I_{cntrl}. There is no way of accurately quantifying the negative contribution of such a peak, since its shape in ω_1 is drawn from a combination of its relaxation properties and its buildup in the solution over the course of the experiment. Such peaks were identified by being proximate to degradation peaks and having a poor fit to the 2-D Gaussian function. We eliminated from the analysis the residues most affected.

Theory. The mathematical theory behind the study of molecular dynamics by NMR has been addressed in detail in many places in the literature (*7*, *23*, *29*, *41*, *42*). Therefore, in this paper we provide just a basic overview of dynamics by NMR, with special attention to the most recent innovations that are important for this study. For a comprehensive review and comparison of approaches, see ref 2.

Analysis of the correlation of the amide bond vector (i.e., N → HN) with its initial orientation as a function of time, $G(t)$, provides information on the dynamics of the protein backbone. For a molecule undergoing isotropic Brownian motion, $G(t)$ decays exponentially. The Fourier transform of $G(t)$ is called the spectral density function, $J(\omega)$, and it indicates the "density" of bond vectors reorienting at any given frequency, ω. $J(\omega)$ has a maximum at $\omega = 0$ and decays as the frequency increases. A rapid decay of $G(t)$ leads to a broad spectral density function, resulting in a reduction of $J(0)$ and an increase of $J(\omega)$ at very high frequencies. In the current study of a large protein at high field, $J(\omega_N)$ varies in parallel with $J(0)$ and opposite from $J(\omega_H)$ when the high-frequency motional component varies.

The shape of the spectral density function of a protein amide relates directly to the relaxation of the ^{15}N nucleus and its attached proton. The most useful measurable relaxation rates are the ^{15}N longitudinal relaxation T_1 (eq 1), transverse relaxation T_2 (eq 2), and heteronuclear $\{^1H\}-^{15}N$ NOE (eq 3) (*43*−*45*), which are determined by the value of the spectral density function $J(\omega)$ at five frequencies: 0, ω_N, ω_H, and $\omega_H \pm \omega_N$.

$$\frac{1}{T_1} = (3D + C)J(\omega_N) + DJ(\omega_{H^-}) + 6DJ(\omega_{H^+}) \quad (1)$$

$$\frac{1}{T_2} = \frac{2(D + C)}{3}J(0) + \frac{3D + C}{2}J(\omega_N) + \frac{D}{2}J(\omega_{H^-}) + 3DJ(\omega_H) + 3DJ(\omega_{H^+}) + R_{EX} \quad (2)$$

$$R_N(H_Z^N \leftrightarrow N_Z) = D[6J(\omega_{H^+}) - J(\omega_{H^-})] \quad (3)$$

$J(\omega_{H^+})$ and $J(\omega_{H^-})$ are shorthand for $J(\omega_H + \omega_N)$ and $J(\omega_H - \omega_N)$, respectively. C and D are evaluated as follows:

$$C = \frac{\Delta^2\omega_N^2}{3} \qquad D = \frac{h^2\gamma_H^2\gamma_N^2}{4r_{NH}^6} \quad (4)$$

where r_{NH} is the internuclear $^{15}N-^1H$ distance, γ_Z is the gyromagnetic ratio for the nucleus Z, $\omega_N = -\gamma_N B_o$, and Δ is the ^{15}N chemical shift anisotropy, for which we used the standard value of −160 ppm (*46*). Since there are five coefficients and only three observed relaxation rates, the solution cannot be determined analytically, and methods have been developed to simplify the problem.

The most common methodology for interpreting relaxation data in proteins has been the model-free approach of Lipari and Szabo (*47*, *48*). But the results from this method are highly dependent upon the estimates of the errors in the peak intensities, which are very difficult to determine accurately. Instead of modeling the dynamics, the relaxation rates can be represented as spectral density values using reduced spectral density mapping (RSDM), which is analytic and independent of error estimates (*24*−*29*, *49*). By assuming that $J(\omega_H) \approx J(\omega_{H^+}) \approx J(\omega_{H^-})$, the value of the spectral density function $J(\omega)$ at three frequencies, $J(0)$, $J(\omega_N)$, and $J(\langle\omega_H\rangle)$, can be calculated using the three relaxation measurements described in eqs 1−3.

$$J(0) = \frac{-3}{4C + 12D}\frac{1}{T_1} + \frac{3}{2C + 6D}\frac{1}{T_2} - \frac{9}{10C + 30D}R_N(H_Z \leftrightarrow N_Z) \quad (5)$$

$$J(\omega_N) = \frac{1}{C + 3D}\frac{1}{T_1} - \frac{7}{5C + 15D}R_N(H_Z \leftrightarrow N_Z) \quad (6)$$

$$J(\langle\omega_H\rangle) = \frac{1}{5D}R_N(H_Z \leftrightarrow N_Z) \quad (7)$$

RSDM marks locations in the molecule where there is motion or chemical exchange that lies outside the range of

the normal motions found virtually everywhere in proteins. Large values of $J(\langle\omega_H\rangle)$ indicate picosecond to nanosecond motion of relatively large amplitude. Chemical exchange processes are indicated by a shorter T_2 and larger $J(0)$ and correspond to alterations in chemical shift on a millisecond to microsecond time scale. While this process often represents the motion of the amide itself, it can also result from nearby motion (especially of an aromatic ring) or binding/release of a ligand, as long as the process produces a chemical shift difference at the nitrogen. Because the total area under the spectral density function is constant (*44*, *50*), an increase in the high-frequency [$J(\langle\omega_H\rangle)$] range will correspond to a decrease in the low-frequency range [$J(0)$ and $J(\omega_N)$]. If one amide undergoes both exchange and very fast motions, the effects on $J(0)$ would tend to cancel, and there may be no indication of the exchange process. However, there would still be an increase in $J(\langle\omega_H\rangle)$ and a decrease in $J(\omega_N)$, which if coupled with an average value of $J(0)$ would point toward a combination of exchange and fast motion. While multiple field strengths can be used to extract the exchange contributions, we did not use them for this study.

Overall Correlation Time. The overall correlation time was determined from the values of $J(0)$ and $J(\omega_N)$ by calculating the second root of the equation:

$$2\alpha\omega_N^2\tau^3 + 5\beta\omega_N^2\tau^2 + 2(\alpha - 1)\tau + 5\beta = 0 \qquad (8)$$

where α and β are functions of $J(0)$ and $J(\omega_N)$. For a complete discussion of this treatment, please see ref 49.

RESULTS AND DISCUSSION

Complete heteronuclear backbone amide assignments of free α-LP and α-LP bound to the boronic acid peptide inhibitor Boc-Ala-Pro-BVal have been previously determined (*31*). The $^{15}N-^{1}H$ correlation spectra at 600 MHz show excellent dispersion; in the spectrum of uncomplexed α-LP all resonances are resolvable except for A116/Q190,[4] which are fully overlapped, and the active site residues G141−S143, which are completely missing. In the spectrum of the complex, all amides are present, but the pairs G6/S18 and T106/N162 are overlapped, and intensity measurements of G35 and I7 are disrupted by side chain amide peaks. Figure 3 displays some time points from a series of T_1 experiments, showing the most crowded region and demonstrating the quality of the spectra. Some representative plots of T_1 and T_2 decays and their best fit single exponential are shown in Figure 4.

Spectral Densities and τ_c. The overall correlation time τ_c was calculated as described above, after first removing all residues with noticeable chemical exchange components in $J(0)$. The resultant values of 8.10 ns (unbound) and 8.14 ns (inhibited) are in the expected range for a compact protein of this size. This negligible difference in τ_c indicates little change in overall structure in solution, as expected from the crystallographic data (substantial differences between bound and free enzymes have been reported for other proteins; see ref 7).

[4] Since there are several different numbering schemes for α-LP, sequential numbering is used throughout this paper to avoid possible confusion. Chymotrypsin homology numbering is given in parentheses when it clarifies a point.

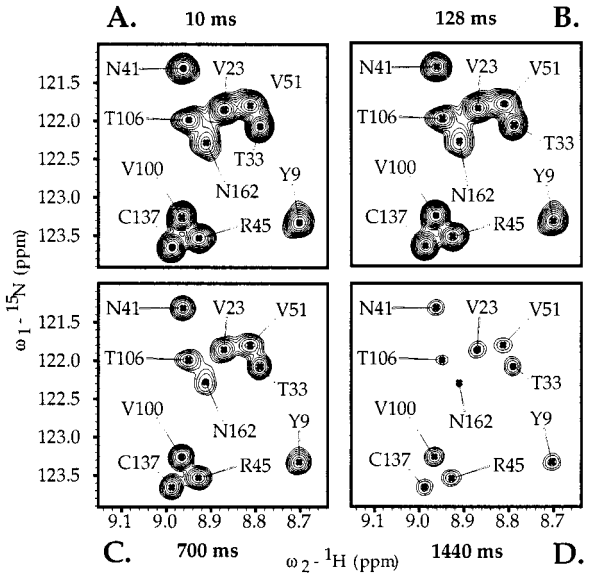

FIGURE 3: Samples of spectra from the T_1 series of free α-LP, showing one of the most overlapped regions. For most peaks, 2-D Gaussian line fits as described in the text were very close to the data. In the region shown, two peaks, Y9 and N162, have slightly distorted shapes and therefore somewhat less perfect fits. The shape imperfections arise from changes in the sample over the course of the experiment, but since all experiments were collected in an arrayed manner, the distortions are consistent throughout. Thus, the Gaussian fits to Y9 or N162 have the same imperfections in each experiment, so the peaks maintain their relative intensities, leading to excellent exponential decay fits to the peak intensities (Figure 4).

Figure 5 shows the spectral densities for the protein sequence, at the three frequencies $J(0)$, $J(\omega_N)$, and $J(\langle\omega_H\rangle)$ for both free and inhibited protease. (The full tables of spectral density values and relaxation rates are available as Supporting Information.) In theory, fast motions should be indicated by a decrease in $J(0)$ and $J(\omega_N)$ and a corresponding increase in $J(\langle\omega_H\rangle)$. However, the RMSD errors of the $J(\langle\omega_H\rangle)$ values are quite large, due to the fact that the heteronuclear NOE experiment is less exact than the T_1 and T_2 relaxation rate determinations. With the exception of a few obvious outliers, the scatter in the $J(\langle\omega_H\rangle)$ values is dominated by random variation, so in most cases these values cannot be used to determine motion. In practice, then, we take a decrease in $J(0)$ and/or $J(\omega_N)$ to suggest fast motion, even in the absence of an increased $J(\langle\omega_H\rangle)$. $J(0)$ and $J(\omega_N)$ are dominated by T_2 and T_1, and these two measurements may be enough for qualitative evaluation of dynamics (see ref 51). The red horizontal lines in Figure 5 correspond to one standard deviation below the mean for $J(0)$ and $J(\omega_N)$; we used this somewhat arbitrary value as a cutoff in determining fast motions, though of course the actual dynamics fall on a continuum. Note that the variation observed in $J(\omega_N)$ and $J(0)$ is almost entirely real, not noise, so the cutoff value is chosen to reflect the amount of motion, not the confidence level. The blue horizontal line in the $J(0)$ plot in Figure 5 represents one standard deviation above the mean and provides a cutoff for nitrogens experiencing intermediate motions or exchange. These 1σ levels would not be appropriate for all proteins but work well in the current study. Table 1 displays pertinent information about the residues with significant dynamics, and regions with significant dynamics are mapped to the molecule in Figure 6.

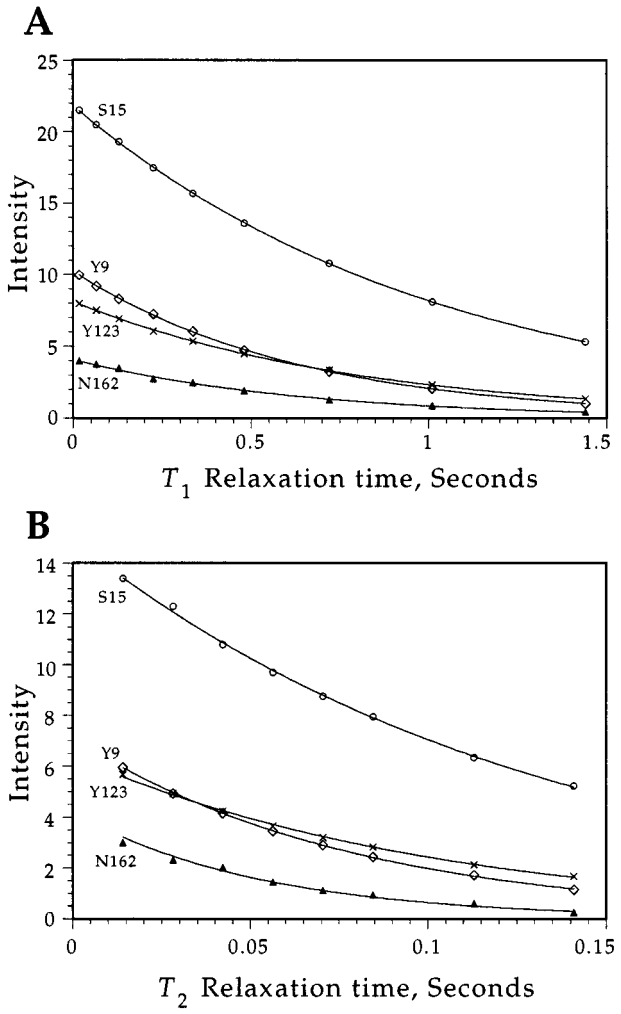

FIGURE 4: Exponential fits to the equation $y = I_o \exp(-t/T_1)$ (or T_2) for several amides in free α-LP. N162 and Y9 have misshapen peaks in the arrayed experiments (see Figure 3), yet their fits are good. (N162 is also among the most overlapped and exchange-broadened.) S15 is undergoing rapid motions, and Y123 undergoes both exchange and rapid motions. As examples of goodness of fit, in T_1, 90% of all amides have fits better than N162, and in T_2, 95% are better than S15. In both cases Y123 is slightly worse than average. The RMSD error is smaller than the shapes used to indicate data points.

Fast Motions. The point on the backbone that has the clearest fast motion is S15 and, to a lesser extent, its neighbor A14. S15 shows a substantially longer T_1 and smaller NOE, which together are positive indicators of fast motion. Most of the other residues with fast motion (Table 1) are well-isolated peaks in the spectra. These residues all reside on the surface of the protein, and most are between or on the edges of secondary structural elements. In addition, except for A98, N122−Y123, and V163, none of the fast motions appear to be stabilized by the presence of the inhibitor, as the spectral density values are similar in the complex. The ease of integration of these isolated peaks, combined with the fact that the results are similar in the complex, increases our confidence that we are indeed detecting dynamics at these locations. Fast motion is indicated by tall pink bands in Figure 5 and red color in Figure 6.

Chemical Exchange. A number of regions show significant increases in $J(0)$, indicating chemical exchange processes on a millisecond to microsecond time scale. They are highlighted by vertical light blue bands (and the blue horizontal line) in Figure 5 and are colored blue in Figure 6. The regions of particular interest are those close to the binding pocket (green trace, bottom of Figure 5), where specificity and binding affinity may be modulated, including R105−G108, N122, A136, G144, and S159−S165. It is especially important to compare the $J(0)$ values of free vs inhibited protein to see what portions of the backbone are stabilized by the peptide inhibitor. Since the boronic acid inhibitor mimics the reaction transition state or nearby tetrahedral intermediate (*20*, *21*), any motions that it stabilizes may have a direct relationship to enzyme activity and/or specificity. Chemical exchange and its stabilization by the inhibitor are indicated in Table 1.

We find that most regions experiencing chemical exchange processes are stabilized in the inhibitor complex, including all those mentioned above except A136. The T106 turn resides directly behind the missing active site residues and displays a fairly uniform $J(0)$ increase. T107 is a broad, weak peak in all spectra of the free enzyme, with an ω_2 (^{1}H) line width almost double the norm, indicating exchange broadening. However, this effect disappears upon inhibitor binding (T106 data are not available in the inhibited spectrum due to overlap). D_2O exchange data show that solvent exchange is not a contributor, nor is the dominant mechanism of exchange likely to be a result of direct interactions with bound peptide, since with the exception of T107 these residues show minor to negligible effects of peptide buildup (see, e.g., G108 in Figure 2). The apparent motion on the millisecond to microsecond time scale that is stabilized by inhibitor binding suggests that this loop is directly involved in binding pocket flexibility. Future experiments involving mutation of these residues may help to illuminate their roles in substrate binding.

Y123 is a particularly interesting case. Its side chain packs against the hydrophobic P_2 site (proline in the inhibitor used here), and it is implicated in stabilizing the S_2 site in the binding pocket through a hydrogen bond network with S159 (*52*). Structural studies of different enzyme−inhibitor complexes showed relatively dramatic shifts in the backbone of Y123 and its neighbors, as well as significant reduction of *B*-factors, upon inhibitor binding (*10*, *12*). Its relaxation properties clearly demonstrate high-frequency motions (through a longer T_1 and altered NOE), which are stabilized by the inhibitor. But the value of $J(0)$ is not as low as would be expected given the increase in $J(\langle\omega_H\rangle)$, so there is probably a contribution from chemical exchange as well, as there is with its neighbor, N122. Motions here may have significance in creating an induced substrate fit, since the P_2 side chain must find a proper orientation next to the tyrosine ring. Of course, the dynamics observed here are backbone, not side chain; accurate assessment of the tyrosine side chain dynamics awaits future studies. We note, however, that reorientation of the Tyr side chain would cause chemical shift changes in local amides. If such a process occurs on a millisecond to microsecond time scale, it would produce exchange broadening in the local amides, which would be reflected in increased values of $J(0)$ (see above). Additional evidence that Y123 undergoes significant chemical exchange, caused by peptide binding, is that it is among those most affected by peptide buildup. The tyrosine ring packs up against the P_2 position of the bound peptide and thus may have multiple conformations as different peptides fit into the binding

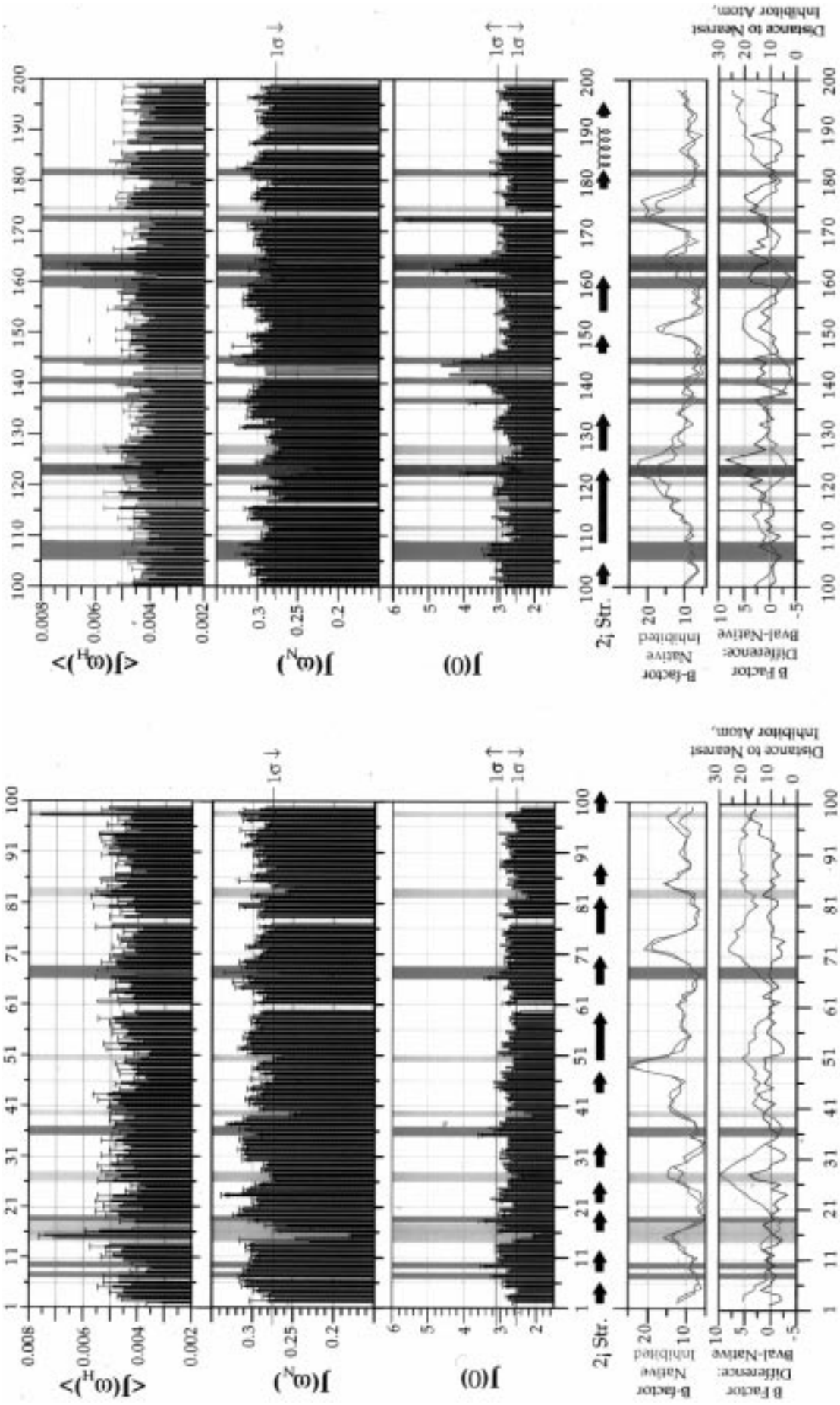

FIGURE 5: RSDM results on the complete sequence of α-LP, both free and inhibited. Values of $J(\omega)$ for the three frequencies are shown by the height of the bars. Black bars are for free α-LP; white and red bars are from the inhibitor complex, with red indicating a substantial change upon inhibitor binding. Vertical stripes highlight regions with substantial dynamic or exchange components (pink = picosecond to nanosecond motions; light blue = chemical exchange). Purple stripes indicate sites involved in both fast motions and exchange (though in both cases, the exchange is at least partly caused by peptide binding). Red and blue horizontal lines indicate that the value is one standard deviation below and above the mean, respectively (after removing the largest outliers), which is the cutoff used to identify motion. *β* strands and the α helix are indicated by arrows and a spring. Uncomplexed crystallographic *B*-factors are indicated by the blue trace near the bottom of the figure, and the inhibited *B*-factors are in red. Below them is shown the difference in *B*-factors (stabilization upon binding) in purple and distance from the amide to the nearest inhibitor atom (Å) in green. Note the correlation between fast motions, secondary structure, and *B*-factor but that such a correlation is much weaker with the chemical exchangers. A few data points are marked in gray—these are locations where overlap or other problems make the data less reliable. To avoid complete visual confusion, error bars were omitted from the data representing the inhibitor complex, but they were of similar magnitude. Error bars on the $\langle J(\omega_H)\rangle$ data represent the standard deviation of the values (after removing outliers), which is the maximum possible error. Since the scatter in the data appears random, not systematic, we feel this is an accurate measure.

Table 1: Characteristics of Dynamic Residues, by Region[a]

residue	motions: fast/slow/both[b]	stabilized by inhibitor?[c]	slow only: nearby aromatics (distance, Å)[d]	slow only: T_2 goodness of fit residual[e]
		Residues Bordering Inhibitor Binding Pocket		
Asn122	both	slow	Y123 (4.8)	**0.900**
Tyr123	both	both	Y123 (3.0); F59 (6.7)	**0.892**
Arg140	slow	slow	H36 (8.9)	**0.995**
Gly144	slow	slow	H36 (5.3); Y9 (6.7); W147 (7.2)	**0.983**
Ser159	slow	slow	H36 (5.3); W147 (5.3); F181 (6.2); Y123 (6.5)	0.998
Gly160	slow	slow	Y123 (4.4); H36 (5.1); W147 (7.0); F181 (7.9)	**0.965**
Asn162	both	??	Y123 (7.5)	**0.756**
Val163	both	slow/fast?	Y123 (8.8)	**0.963**
Gln164	slow	slow	Y123 (12.1)	**0.980**
		Residues in Region of Binding Pocket		
Gly35	slow	??	H36 (5.1); F59 (5.6); F54 (5.8)	0.986
His36	slow		H36 (3.2); F59 (3.8); F54 (6.4); Y123 (7.8)	**0.987**
Thr107	slow	slow	Y109 (9.7)	0.911
Gly108	slow	slow	Y109 (7.3)	**0.998**
Thr120	fast			
Gly126	fast			
Ala127	fast			
Ile172	slow (strong)	slow, partial	W147 (14.2)	0.998
Phe181	slow		F181 (3.2); W147 (5.1)	**0.995**
		Residues That Bind Substrate on C-Terminal Side of Cleavage Point		
Ala14	fast			
Ser15	fast (strong)			
Leu16	fast?			
Ser18	slow	??	Y9 (3.6); F31 (6.9)	**0.997**
Arg105	slow	slow	Y9 (8.7)	**0.992**
Thr106	slow	??	Y9 (10.7)	**0.973**
		Other Residues with Significant Dynamic Behavior		
Ile7	slow	??	Y9 (6.9)	0.998
Tyr9	slow	slow	Y9 (3.2); F31 (6.7)	**0.998**
Cys17	fast?			
Gly26	fast			
Ala27	fast			
Thr39	fast			
Val50	fast			
Trp66	slow	slow	W66 (3.3); Y191 (4.7); F54 (5.2); F31 (7.0)	0.998
Gly82	fast			
Ser83	fast			
Ala95	fast			
Val96	fast?			
Ala98	fast			
Ala99	fast			
Cys111	fast			
Lys117	fast			
Ala136	slow		W147 (4.5)	**0.998**
Ala174	fast			

[a] Table provides information on only those residues with significant dynamics according to the parameters described in the text and in Figure 5. Residues are grouped according to their relation to the binding pocket. [b] Question mark denotes borderline or somewhat ambiguous data, but probable candidate. [c] Which motion(s), if any, are significantly stabilized by the bound inhibitor. Question marks indicate residues where inhibitor data were too overlapped to accurately measure. [d] Crystal structure distance, in angstroms, between amide nitrogen and nearest heavy atom of nearest aromatic ring and of other aromatic rings that are within 8.0 Å. Shorter distances increase the chance that aromatic ring motion could be causing chemical exchange, through changing ring current shifts. [e] Goodness of fit (R) from least-squares fit to T_2 data, when the data were collected in complete experiments in mixed-up order. A poor fit (lower R) may be caused by the changes in the sample over the 24 h of data collection (see Figure 2 and discussion in text). High R suggests that chemical exchange is caused primarily by motion, while lower R indicates that at least part of the $J(0)$ derives from binding and release of proteolytic products. Boldface indicates that the characteristic pattern above and below the fit (as seen in Figure 2) was observed; lightface means the variation was random (and therefore not caused byproduct binding). R values were calculated from simple exponential fits, using the Macintosh program KaleidaGraph.

pocket. This would explain the strong chemical exchange component, associated with breakdown products, seen in most of the nearby amides (Y123, N122, D125, and G161; see Figure 6A and Table 1).

G160 and G161 are in a strand that runs antiparallel to the inhibitor, forming one side of the binding pocket. The side chain of V163 provides interactions that help to mediate specificity of the P_1 substrate residue (*13*). These residues are seen to change conformation in different crystal structures in order to accommodate different P_1 side chains (see Figure 1). Overall, this is confirmed by the spectral densities—there are strong indications of both slow and fast motions in the region, and all are stabilized by the inhibitor. (N162 is degenerate with T106 in the inhibited spectrum, so nothing can be determined about its stabilization.) We suspect that peptide binding plays a substantial role in the exchange term

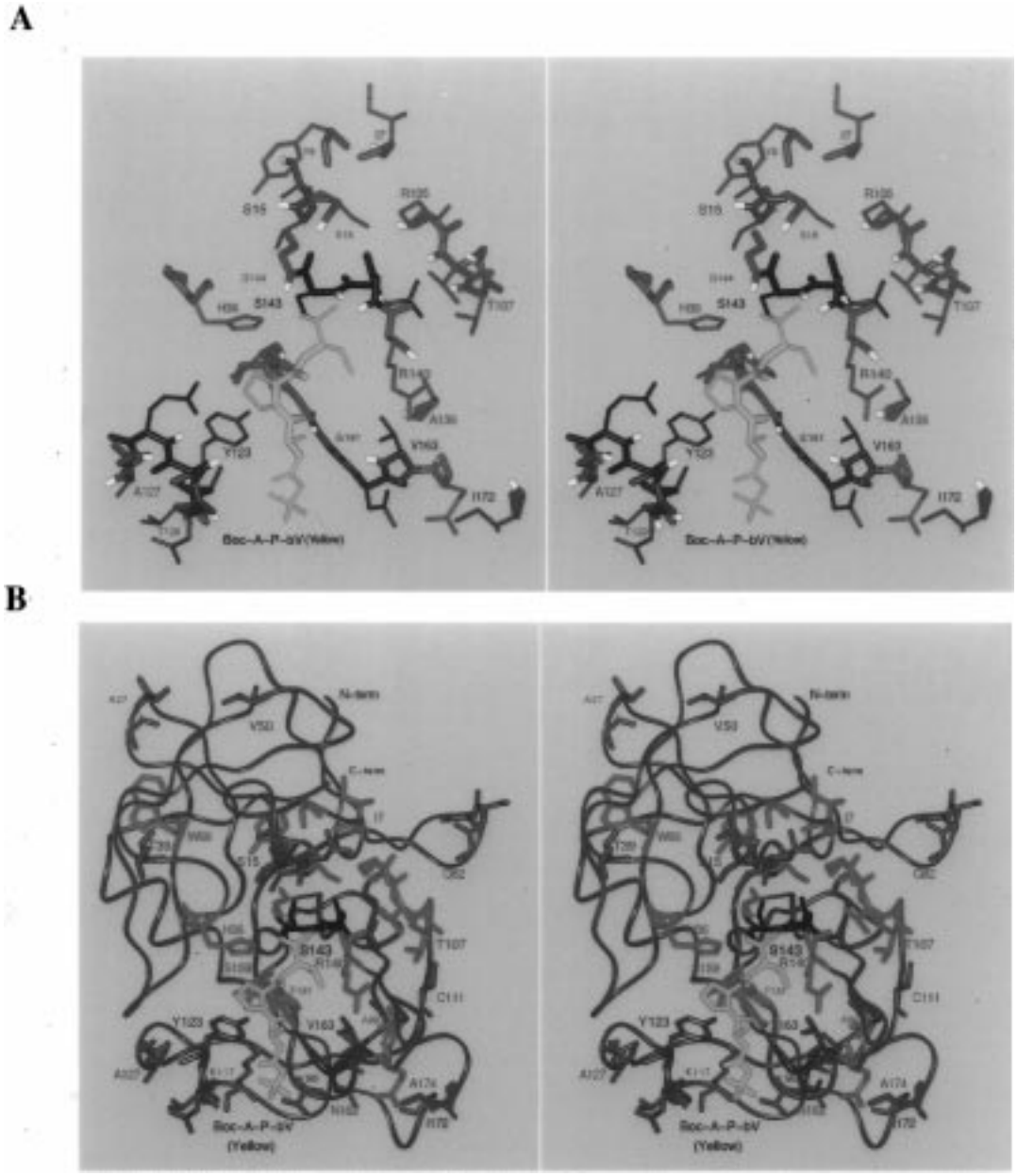

FIGURE 6: "Relaxed eye" stereoviews of α-LP, showing the dynamics and the bound inhibitor. Red indicates fast motions and blue, chemical exchange. I172 is in green; it has a large chemical exchange component, partially stabilized by the inhibitor but not at all affected by peptide binding. This residue plays an unknown but important role in mediating substrate specificity. The three missing active site residues, G141−S143, are in black, and the inhibitor is in yellow. Purple residues have both fast and slow motions; of these, N122, Y123, and G161 have large chemical exchange contributions from peptide binding. These residues all reside near the ring of Y123, which may reorient upon peptide binding. V163 and Q164 have moderate contributions from peptide binding. (A) Detail of the binding region. Amide hydrogens are in white. Note the hydrogen bond formed between G161 and the inhibitor, serving to stabilize the glycine pair. Y123 and G161−V163 also apparently undergo rapid motions, which could allow recognition of different side chains in the P_2 and P_3 positions. (B) View of the entire molecule, with dynamic and exchanging residues colored. Note that the residues in fast motion (red) are all on the outside of the molecule, generally outside of secondary structural elements.

because the whole stretch G160−Q164 is significantly affected by peptide buildup (see, e.g., G160 in Figure 2). But there is also a puzzle—G161 appears to be among the most flexible residues in the crystal structure superpositions (see Figure 1) and does not have any strong hydrogen bonds or side chain interactions to hold it in place, so it would appear to be an excellent candidate for dynamic behavior. Its ^{1}H line width is broadened about 50%, and its ^{15}N line width about 15%, in unbound HSQC spectra, which indicates chemical exchange. Furthermore, it is among those most affected by peptide buildup. Yet its spectral densities $J(0)$ and $J(\langle\omega_H\rangle)$ are singularly average, in contrast with its neighbors, implying that it is relatively stable. This apparent contradiction can be explained if G161 is undergoing fast motions and chemical exchange simultaneously, which have opposite effects on $J(0)$. The moderately reduced value for $J(\omega_N)$ supports this hypothesis. Since the peak is weak, and therefore the NOE intensity measurements not as accurate, the value for $J(\langle\omega_H\rangle)$ would have even greater than normal uncertainty, so its slightly low value has less significance. The values found in the complex should be accurate, since the line broadening is completely removed and all other neighbors are stabilized. G161 has been the target of extensive mutagenesis (*16*), and crystallographic data indi-

cated that certain substitutions resulted in reduced flexibility. Future NMR studies of the dynamics of these mutations will be illuminating.

Interestingly, I172 shows a greatly increased $J(0)$ that is partially stabilized by the inhibitor. Yet there is absolutely no effect on T_2 from peptide buildup. Its position on the surface >10 Å from the nearest inhibitor atom might suggest a lack of significance for substrate binding. However, it is part of a loop that has been intensively studied by scanning alanine mutagenesis by Mace et al. (*15*), who discovered that I172 plays a surprisingly large role in modulating the activity of the enzyme to a variety of substrates. The motion detected in this study suggests that there is a dynamic as well as functional coupling between this distant residue and the binding pocket. Future experiments on the mutants will help us to understand the role played by dynamics in the mechanism connecting I172 to substrate binding.

P_1' and P_2' Sites. While the inhibitor used in this study had no extension beyond the scissile bond, a crystallographic study with a peptide phosphonate inhibitor provided evidence for how activity and specificity may be modulated by contacts made in the P_1' and P_2' sites (*14*). The crystal structure revealed that two hydrogen bonds are formed between the phosphonate transition state analogue and L16 in the enzyme. L16 appears to have a moderate but significant high-frequency component [from its low $J(\omega_N)$], possibly combined with chemical exchange terms [from its higher $J(0)$], and it is adjacent to S15, the residue with the largest high-frequency motions in the entire protein. The side chain of P_1' contacts S15, and the P_2' side chain sandwiches between the side chains of L16 and T106, a residue in slow exchange. Thus, the motion of these regions may be important to allow broad specificity in the residues beyond the scissile bond—a high degree of specificity for those residues would make cleavage of a random peptide sequence rather unlikely. Dynamics studies of phosphonate ester complexes or of peptides bound to enzymes with mutated active sites may help to determine the role that flexibility of these P_1' and P_2' contact sites plays in substrate binding.

Aromatic Rings. Constantine et al. (*53*) found correlations between residues undergoing chemical exchange and proximity to aromatic rings. Since chemical exchange may be due to any process that alters chemical shift, an aromatic ring that changes its orientation (i.e., not just a ring flip) would usually perturb the chemical shifts of nearby nuclei through ring current shifts. We examined the crystal structure for evidence of such a correlation. Table 1 includes, for all slow exchangers, the crystal structure distance between the amide nitrogen and the nearest ring heteroatom and other nearby rings if within 8 Å. It is clear that some amides are far from any aromatic ring (e.g., I172 and T106) while others are close. But one would expect that if a ring were moving, it would affect most of the nearby amides. The only rings that are close to several of the amides in slow exchange are Y9, H36, and Y123. Of these, only Y123 has ring carbon crystallographic *B*-factors that are at all elevated. We conclude from this that ring current shifts might possibly contribute to the binding pocket exchange, and conceivably to several other places, but do not significantly contribute to the majority of the observed chemical exchange.

Comparison with Crystallographic B-Factors. The crystal structures of free α-LP (*8*) and the complex with the Boc-Ala-Pro-BVal inhibitor (*10*) have both been determined to high resolution. To avoid autolysis, a protease might be expected to show reduced breathing motions and a highly cooperative unfolding transition. For well-determined structures, the crystallographic *B*-factors provide information on both time-averaged dynamical properties as well as static disorder in the crystal. Because of the combination of terms in the crystallographic *B*-factors, comparison with NMR dynamics data can be informative. As shown in Figure 5, the backbone nitrogen *B*-factors are quite low, averaging around 10 and rarely exceeding 15. Previous studies comparing solution dynamics with crystallographic *B*-factors have shown everything from a good correlation (*40*) to a moderate correlation (*54*) to no correlation at all (*42*, *53*, *55*). This study joins the middle range with moderate but not complete correlation, better on the high-frequency motions and worse on the exchange processes.

Most of the fast-moving amides are located on surface loops between secondary structural elements, and all except G82 and C111 are associated with above average *B*-factors. In the three instances where fast motions are stabilized by inhibitor binding (A98, Y123, and V163), the *B*-factor is also significantly reduced upon inhibitor binding, suggesting that a portion of the *B*-factor is caused by the motion of the nitrogen observed in solution. Note, however, that while the fast motion observed by NMR in this study is generally associated with increased *B*-factors, high *B*-factors do not necessarily correspond with NMR-observed motions (the best examples are found around A72 and S150). This is not unexpected, since heteronuclear relaxation is affected by motion over rather limited frequency ranges, while high *B*-factors can be caused by motions at any time scale and also by crystal packing interactions or static disorder within the crystal.

There is a poorer correlation between regions of chemical exchange (blue bars) and *B*-factor, as has been seen elsewhere (*53*). In some instances (e.g., N122 and I172) there is a clear relationship. Yet many other sites with exchange terms appear at a nadir in the *B*-factor trace. R105−G108, for instance, have low *B*-factors and no proximate aromatic rings, yet show strong exchange activity. Since this stretch is near the active site, future studies with mutations or different inhibitors may shed light on the exchange mechanism. Here we must reemphasize that chemical exchange does not necessarily imply dynamics of the amide, so a perfect correlation would not be expected. Since we believe that many of the binding pocket residues derive much of their chemical exchange contribution from peptide exchange, the lack of a strong correlation is not surprising.

Recently, Rader and Agard (*9*) reported the low temperature (120 K) crystal structure of α-LP to determine the contribution of dynamics to the observed *B*-factors. At low temperature one would expect simple thermal motion, and the corresponding *B*-factors, to be reduced to low values, while more complex motions involving multiple minima may be trapped in multiple states and be modeled by an increased *B*-factor. To better understand the nature of these states frozen out at low temperatures, the cryocrystallography study

used multiple conformation refinement to more correctly model the conformations of these states.

Overall there is a good, though not perfect, correlation between the results of NMR and of low-temperature crystallography. As an example of simple thermal motion, the region around T120 has many amides in fast motion by NMR and displays the largest change in *B*-factor upon temperature reduction. Perhaps more importantly, multiple conformational states were observed in residues around the binding pocket and were suggestive of long-range correlated motions. The existence of such multiple conformations at low temperature implies the presence of kinetic barriers between states. The same barriers may exist at room temperature and be responsible for motions on the millisecond to microsecond time scale. Thus, they could appear in NMR studies as intermediate exchange, and the significant exchange terms in residues near V163, and also in R140, are consistent with such a picture.

Dynamics and Specificity. The observed pattern of dynamics reveals that the most flexibility occurs at sites contacting the bound substrate, but away from the cleavage point. The binding pocket is generally in motion, but the region directly around the catalytic site (e.g., S18, R140, G145, G139, and G144) shows only moderate to negligible chemical exchange, while sites that bind either the P_2 position (e.g., Y123) or the P_1' and P_2' residues (e.g., S15 and T106) have strong chemical exchange and/or high-frequency components. It is interesting that some of the greatest dynamic flexibility appears in the region that contacts the P_2 site. Flexibility there may be necessary to allow many different sequences to be accommodated, leaving specificity to be determined only by the P_1 position. The low-temperature crystal structure results discussed above (*9*), as well as the earlier inhibitor studies (*10*, *12*), support this conclusion.

CONCLUSIONS

We have used ^{15}N NMR relaxation experiments to determine the values of the spectral density function at three frequencies, $\langle\omega_H\rangle$, ω_N, and 0, for α-lytic protease, both free and in complex with the boronic acid inhibitor Boc-Ala-Pro-BVal. Our results, when mapped to the molecule (Figure 6), indicate that there are regions undergoing rapid motions (nanosecond to picosecond), most of which are not stabilized by the inhibitor, and other regions experiencing chemical exchange processes, at least some of which imply relatively slow (millisecond to microsecond) motions of the corresponding amide bonds. Most of the exchange processes occur close to the binding pocket and are stabilized by inhibitor binding. A few residues adjacent to the binding site (e.g., Y123 and V163) appear to relax by both fast and slow processes and may be involved in determining the specificity of the enzyme. Another known specificity determinant, I172, is located more than 10 Å from the inhibitor and was hypothesized to be involved in modulating flexibility at the binding pocket (*15*). Intriguingly, I172 appears to be moving substantially on a millisecond to microsecond time scale, suggesting that I172 dynamics may be important for modulating specificity. In general, the locations with fast motions tend to correlate with high *B*-factors and to fall between secondary structural elements. However, there are sufficient discrepancies such that the overall correlation between *B*-factor and solution dynamics is only moderate.

Proteins are constantly sampling conformational space and spend time in the various kinetically accessible states according to their kinetic and thermodynamic equilibrium relationships. We know from crystallographic studies that the binding pocket of α-LP can adopt different conformations in order to accommodate different substrates. If in the unbound enzyme all of these conformations exist with reasonable probability in thermodynamic equilibrium, then there would be dynamic behavior in the binding pocket which could be detectable by NMR. In particular, one would expect to detect the largest dynamic effect where the enzyme has to make the largest adjustments to accommodate the various substrates. The pattern of spectral densities suggests that dynamics do play a role in determining patterns of substrate specificity. Given its presumed biological role in hydrolyzing proteins as a source of nutrient amino acids, broad substrate specificity outside of the P_1 position should be desirable while excessive flexibility at P_1 would likely reduce k_{cat}. The residues with the strongest dynamic components in both frequency ranges are near the bound substrate but removed from the substrate cleavage point. Such backbone motion may allow the enzyme to conform itself to many different substrate sequences, aside from the P_1 substrate residue. An efficient enzyme also needs reasonable substrate on−off rates, yet must have structural stability during catalysis. That most of the binding pocket residues experience chemical exchange stabilized by inhibitor binding suggests that the binding pocket is flexible to admit substrate, but rigidifies upon substrate binding, to maximally stabilize the transition state. The less flexible active site residues also help to impart specificity and stabilize the transition state. In particular, Y123 motion may facilitate substrate access and exit, since it is located near the center of the binding pocket.

We have demonstrated the utility of reduced spectral density mapping for studying protein dynamics in α-LP. In contrast to the "model-free" approach, RSDM greatly simplifies the interpretation of experimental dynamics data without requiring a particular motional model. With the model-free method, the RMS errors in the measured relaxation rates are critical for choosing how many and which parameters are necessary for a fit, and we have found that these errors can be very difficult to estimate accurately for all residues. With RSDM, errors only affect the deviations of the spectral density function values but do not change the model used. Thus it is less sensitive to the kinds of imperfections found in spectra from overlap, impurities, side chain peaks, etc., all of which can affect the accuracy of individual relaxation rates. This is especially critical in making an assessment of contribution of chemical exchange. We feel that RSDM will be very useful in future studies of protein dynamics.

These results represent a first step in the analysis of the relationship between dynamics, structure, and function of α-LP using NMR. The full picture will not emerge until studies are completed on carefully chosen mutants and different inhibitors. In addition, side chain dynamics studies will be very useful in probing the role motion may play among the various components of the binding pocket that make many of the enzyme−substrate contacts. However, even at this stage, it appears that the observed patterns of

enzyme specificity are not dictated solely by the properties of the residues in immediate contact with substrate; instead, they result from more deeply imbedded dynamic properties of the molecule as a whole.

ACKNOWLEDGMENT

The authors thank Drs. Dennis Benjamin and Art Palmer for useful discussions, Dr. Lewis Kay for kindly providing pulse sequence code, Drs. Don Kneller and Yoko Haga for programming help, Dr. Vladimir Basus for technical assistance, and Dr. Charles Kettner for kindly providing the Boc-Ala-Pro-BVal. Dr. Kwaku Dayie receives special thanks for his help with RSDM, and thanks also to Drs. Gerhard Wagner and Stephen Rader for critical reading of the manuscript.

SUPPORTING INFORMATION AVAILABLE

One table of the relaxation rates and NOE values of free and inhibited α-LP and a table of the spectral density values (12 pages). Ordering information is given on any current masthead page.

REFERENCES

1. Williams, R. J. P. (1989) *Eur. J. Biochem. 183*, 479−497.
2. Dayie, K. T., Wagner, G., & Lefèvre, J.-F. (1996) *Annu. Rev. Phys. Chem. 47*, 243−282.
3. Bennett, W. S., & Huber, R. (1984) *CRC Crit. Rev. Biochem. 15*, 291−384.
4. Hodsdon, M. E., and Cistola, D. P. (1997) *Biochemistry 36*, 2278−2290.
5. Akke, M., Skelton, J. H., Kordel, J., Palmer, A. G., III, and Chazin, W. J. (1993) *Biochemistry 32*, 9832−9844.
6. Nicholson, L. K., et al. (1992) *Biochemistry 31*, 5253−5263.
7. Farrow, N. A., et al. (1994) *Biochemistry 33*, 5984−6003.
8. Fujinaga, M., Delbaere, L. T. J., Brayer, F. D., and James, M. N. G. (1985) *J. Mol. Biol. 183*, 479−502.
9. Rader, S. D., and Agard, D. A. (1997) *Protein Sci. 6*, 1375−1386.
10. Bone, R., Shenvi, A. B., Kettner, C. A., and Agard, D. A. (1987) *Biochemistry 26*, 7609−7614.
11. Bachovchin, W. W., Wong, W. Y. L., Farr-Jones, S., Ashok, B. S., and Kettner, C. A. (1988) *Biochemistry 27*, 7689−7697.
12. Bone, R., Frank, D., Kettner, C. A., and Agard, D. A. (1989) *Biochemistry 28*, 7600−7609.
13. Bone, R., Fujishige, A., Kettner, C. A., and Agard, D. A. (1991) *Biochemistry 30*, 10388−10398.
14. Bone, R., Sampson, N. S., Bartlett, P. A., and Agard, D. A. (1991) *Biochemistry 30*, 2263−2272.
15. Mace, J. E., Wilk, B. J., and Agard, D. A. (1995) *J. Mol. Biol. 251*, 116−134.
16. Mace, J. E., and Agard, D. A. (1995) *J. Mol. Biol. 254*, 720−736.
17. Sohl, J. L., and Agard, D. A.. (1995) in *Intramolecular Chaperones and Protein Folding* (Shinde, U., and Inouye, M., Eds.) pp 62−83, R. G. Landes Co., Austin, TX.
18. Silen, J. L., Frank, D., Fujishige, A., Bone, R., and Agard, D. A. (1989) *J. Bacteriol. 171*, 1320−1325.
19. Baker, D., Sohl, J. L., and Agard, D. A. (1992) *Nature 356*, 263−265.
20. Kettner, C. A., and Shenvi, A. B. (1984) *J. Biol. Chem. 259*, 15106−15114.
21. Kettner, C. A., Bone, R., Agard, D. A., and Bachovchin, W. W. (1988) *Biochemistry 27*, 7682−7688.
22. Wagner, G. (1993) *Curr. Opin. Struct. Biol. 3*, 748−754.
23. Farrow, N. A., Zhang, O., Forman-Kay, J. D., and Kay, L. E. (1997) *Biochemistry 36*, 2390−2402.
24. Farrow, N. A., Zhang, O., Forman-Kay, J. D., and Kay, L. E. (1995) *Biochemistry 34*, 868−878.
25. Farrow, N. A., Zhang, O., Szabo, A., Torchia, D. A., and Kay, L. E. (1995) *J. Biomol. NMR 6*, 153−162.
26. Wagner, G. (1994) Approaches for Studies of Protein Mobility and Structure, 35th Experimental Nuclear Maganetic Resonance Conference, April 10−15, 1994, Asilomar, CA.
27. Ishima, R., and Nagayama, K. (1995) *Biochemistry 34*, 3162−3171.
28. Ishima, R., and Nagayama, K. (1995) *J. Magn. Reson., Ser. B 108*, 73−76.
29. Peng, J. W., and Wagner, G. (1995) *Biochemistry 34*, 16733−16752.
30. Hunkapiller, M. W., Smallcombe, S. H., Whitaker, D. R., and Richards, J. H. (1973) *Biochemistry 12*, 4732−4743.
31. Davis, J. H., Agard, D. A., Handel, T. M., and Basus, V. J. (1997) *J. Biomol. NMR 10*, 21−27.
32. Grzesiek, S., and Bax, A. (1993) *J. Biomol. NMR 3*, 185−204.
33. Logan, T. M., Olejnickzak, E. T., Xu, R. X., and Fesik, S. W. (1993) *J. Biomol. NMR 3*, 225−231.
34. Davis, J. H. (1995) *J. Biomol. NMR 5*, 433−437.
35. Sklenar, V., Torchia, D. A., and Bax, A. (1987) *J. Magn. Reson. 73*, 375.
36. Delaglio, F., et al. (1995) *J. Biomol. NMR 6*, 277−293.
37. Delaglio, F. (1993) NMRPipe Software System, National Institutes of Health, Bethesda, MD.
38. Press, W. H., Flannery, B. P., Teukolsky, S. A., and Vertterlinh, W. T. (1988) *Numerical Recipes in C—The Art of Scientific Computing*, Cambridge University Press, New York.
39. Palmer, A. G., III, Rance, M., and Wright, P. E. (1991) *J. Am. Chem. Soc. 113*, 4371−4380.
40. Kördel, J., Skelton, J. J., Akke, M., Palmer, A. G., III, and Chazin, W. J. (1992) *Biochemistry 31*, 4856−4866.
41. Clore, G. M., et al. (1990) *J. Am. Chem. Soc. 112*, 4989−4991.
42. Kay, L. E., Torchia, D. A., and Bax, A. (1989) *Biochemistry 28*, 8972−8979.
43. Markus, M., Dayie, K., Matsudaira, P., and Wagner, G. (1996) *Biochemistry 35*, 1722−1732.
44. Abragam, A. (1961) *The Principles of Nuclear Magnetism*, Clarendon Press, Oxford, England.
45. Peng, J. W., and Wagner, G. (1992) *Biochemistry 31*, 8571−8586.
46. Hiyama, Y., Niu, C., Silverton, J. V., Bavaso, A., and Torchia, D. A. (1988) *J. Am. Chem. Soc. 110*, 2378−2383.
47. Lipari, G., and Szabo, A. (1982) *J. Am. Chem. Soc. 104*, 4546−4559.
48. Lipari, G., and Szabo, A. (1982) *J. Am. Chem. Soc. 104*, 4559−4570.
49. Lefèvre, J.-F., Dayie, K. T., Peng, J. W., and Wagner, G. (1996) *Biochemistry 35*, 2674−2686.
50. Ernst, R. R., Bodenhausen, G., and Wokaun, A. (1987) *Principles of Nuclear Magnetic Resonance in One and Two Dimensions*, Oxford University Press, Oxford, England.
51. Habazettl, J., and Wagner, G. (1995) *J. Magn. Reson. 109*, 100−104.
52. Epstein, D. M., and Abeles, R. H. (1992) *Biochemistry 31*, 11216−11223.
53. Constantine, K. L., et al. (1993) *Proteins 15*, 290−311.
54. Clore, G. M., Driscoll, P. C., Wingfield, P. T., and Gronenborn, A. M. (1990) *Biochemistry 29*, 7387−7401.
55. Stone, M. J., Chandrasekhar, K., Holmgren, A., Wright, P. E., and Dyson, H. J. (1993) *Biochemistry 32*, 426−435.

BI972963P